Acta Crystallographica Section D
Biological Crystallography
ISSN 0907-4449

The structures of *Alcaligenes faecalis* D-3-hydroxybutyrate dehydrogenase before and after NAD^+ and acetate binding suggest a dynamical reaction mechanism as a member of the SDR family

Md Mominul Hoque,[a] Satoru Shimizu,[a] Md Tofazzal Hossain,[a,b] Tamotsu Yamamoto,[c] Shigeyuki Imamura,[c] Kaoru Suzuki,[d] Masaru Tsunoda,[d] Hitoshi Amano,[e] Takeshi Sekiguchi[d] and Akio Takénaka[a,d]*

[a]Graduate School of Bioscience and Biotechnology, Tokyo Institute of Technology, 4259 Nagatsuta-cho, Midori-ku, Yokohama, Kanagawa 226-8501, Japan, [b]Department of Biochemistry and Molecular Biology, University of Rajshahi, Rajshahi 6205, Bangladesh, [c]Asahi Kasei Pharma Corporation, Tagat-gun, Shizuoka 410-2323, Japan, [d]College of Science and Engineering, Iwaki Meisei University, Chuodai-iino, Iwaki 970-8551, Japan, and [e]Fukushima National College of Technology, Taira-kamiarakawa, Iwaki 970-8034, Japan

Correspondence e-mail: atakenak@bio.titech.ac.jp

Received 14 December 2007
Accepted 7 February 2008

PDB References:
D-3-hydroxybutyrate dehydrogenase, 2yz7, r2yz7sf; complex with NAD^+ and acetate, 2zea, t2zeasf.

D-3-Hydroxybutyrate dehydrogenase, which catalyzes the reversible reaction between D-3-hydroxybutyrate and acetoacetate, has been classified into the short-chain dehydrogenase/reductase family and is a useful marker in the assay of diabetes mellitus and/or ketoacidosis. The enzyme from *Alcaligenes faecalis* was crystallized in the apo form and in the holo form with acetate as a substrate analogue. The crystal structures of both forms were determined at 2.2 Å resolution. The enzyme is a tetramer composed of four subunits assembled with noncrystallographic 222 point symmetry. Each subunit has two domains. The principal domain adopts the Rossmann fold essential for nucleotide binding, which is a common feature of the SDR family. NAD^+ is bound in a large cleft in the domain. The pyrophosphate group of NAD^+ is covered by the small additional domain, which is supported by two extended arms allowing domain movement. In the catalytic site, a water molecule is trapped by the catalytic Tyr155 and Ser142 residues in the vicinity of the bound NAD^+ and acetate. The substrate analogue acetate is bound above the nicotinamide plane. A substrate (D-3-hydroxybutylate) bound model can reasonably be constructed by adding two C atoms into the void space between the water O atom and the methyl group of the acetate, suggesting a substrate-bound state before enzymatic reaction occurs. Based on these structural features, a reaction mechanism has been proposed.

1. Introduction

Acetyl-CoA formed by fatty-acid degradation has two fates: the normal oxidation of acetyl-CoA *via* the citric acid cycle and the formation of acetoacetate and 3-hydroxybutyrate under low-carbohydrate conditions. Acetoacetate, 3-hydroxybutyrate and acetone are collectively referred to as ketone bodies; acetone is a nonmetabolizable decarboxylation product of acetoacetate. These ketone bodies are energy-rich compounds that transport energy from the liver to other tissues (Laffel, 1999). During periods of glucose deficiency, ketone bodies are used as an alternative source of energy (Francois *et al.*, 1981; Randle *et al.*, 1964). Unlike most other tissues, the brain cannot utilize fatty acids for energy when blood glucose levels become compromised. In this case, ketone bodies are an alternative source of energy in the brain, amounting to nearly two-thirds of the total brain energy necessary duing periods of prolonged fasting and starvation (Laffel, 1999). Ketone bodies stimulate insulin release *in vitro* (Ikeda *et al.*, 1987; Malaisse *et al.*, 1990), generate oxygen radicals and cause lipid peroxidation (Jain *et al.*, 1998).

Although ketone bodies are important energy sources, excess levels cause ketoacidosis. In this situation, a potentially life-threatening metabolic acidosis occurs through the high amounts of protons provided by acetoacetate and hydroxybutyrate, which exceed the serum bicarbonate buffer capacity. Serum levels of 5–10 m*M* ketone bodies are reached under these circumstances, compared with levels of 1 m*M* in normal states. Peripheral tissues take up ketone bodies and oxidize hydroxybutyrate back to acetoacetate, which is then ultimately converted into acetyl-CoA, entering the tricarboxylic acid cycle. Diabetes is the most common pathological case of high ketone concentrations in the blood, which leads to unconsciousness and coma.

D-3-Hydroxybutyrate dehydrogenase (HBDH; EC 1.1.1.30) is an NAD^+-dependent enzyme that catalyzes the reversible reaction between D-3-hydroxybutyrate and acetoacetate (Fig. 1). HBDH is of special interest because the reaction that it catalyzes is a useful basis for a rapid and specific method for the determination of the ketone bodies acetoacetate and hydroxybutyrate, which are an important parameter in the diagnosis and monitoring of insulin-dependent diabetes mellitus (type I; Kruger *et al.*, 1999). In order to reveal the reaction mechanism of HBDH, we initiated X-ray analysis of the enzyme from *Alcaligenes faecalis* (*Af*-HBDH) and of its complex with NAD^+ and acetate as a substrate analogue, as the three-dimensional structure was not known. Recently, the crystal structures of HBDH from *Pseudomonas fragi* (*Pf*-HBDH; Ito *et al.*, 2006) and of a human cytosolic type II HBDH (DHRS6; Guo *et al.*, 2006) have been reported. We considered HBDH to be a type of alcohol dehydrogenase, even though its substrate is a carboxylic acid. HBDH belongs to a large family of short-chain dehydrogenase/reductases (SDRs), also known as the short-chain oxidoreductase (SCOR) family (Jörnvall *et al.*, 1995), that are found in humans, mammals, insects and bacteria. SDRs have a wide variety of substrate specificities that range from simple alcohols to complex compounds such as steroids, prostaglandins, sugars and xenobiotics (Tanaka *et al.*, 2001). At present, well over 4000 members have been deposited in sequence databases and about 50 three-dimensional structures corresponding to 20–30 distinct enzymatic activities are available (Jörnvall *et al.*, 1995; Kallberg *et al.*, 2002; Oppermann *et al.*, 2003). The sequence identity in pairwise comparisons of different SDR enzymes is typically 15–30%, but all the available three-dimensional structures exhibit a highly similar α/β folding pattern with a Rossmann fold. The most variable parts of the SDR structures are the substrate-binding regions. Remarkably, the oxidoreductases of the SDR family vary greatly with respect to the substrate on which they act, but the basic mechanism of hydride transfer is the same from the most simple case of alcohol to more complex substrates. In order to understand this enormous diversity, it would be of great interest to investigate the three-dimensional structure, catalytic mechanism, coenzyme specificity and substrate specificity of the SDR enzymes. This paper not only describes the structural details of *Af*-HBDH that differ from those of the previously reported *Pf*-HBDH and human DHRS6 structures, but also proposes a dynamical reaction mechanism. In addition, the evolutionary relationship and possible roles of the residues that are conserved in the short-chain dehydrogenase/reductase family are discussed.

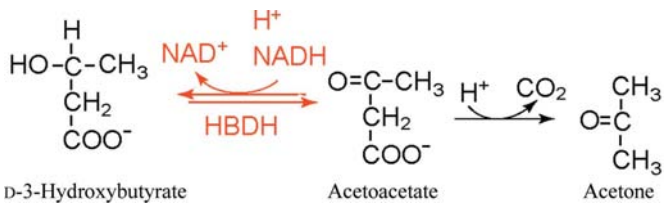

Figure 1
HBDH catalyzes the reversible reaction between D-3-hydroxybutyrate and acetoacetate. Acetoacetate is spontaneously decarboxylated to acetone.

2. Materials and methods

2.1. Enzyme expression and purification

A plasmid harbouring the *Af*-HBDH gene was introduced into the expression host *Escherichia coli* DH1. Cells were grown for 20 h at 310 K in BHI medium and were collected by centrifugation at 7000*g* for 10 min. Pellets were suspended in Tris–HCl buffer pH 8.5 containing 0.2% lysozyme. The cell suspension was incubated at 310 K for 2 h with continuous stirring. The supernatant obtained by centrifugation at 7000*g* for 20 min was loaded onto a Q-Sepharose FF column. The enzyme was eluted with a linear gradient of 0–0.3 *M* KCl in 10 m*M* Tris–HCl buffer pH 8.5. Ammonium sulfate (20%) was added to the pooled enzyme fractions. The fractions were applied onto a Phenyl-Sepharose FF column and the adsorbed enzyme was eluted with a linear gradient of 20–0% ammonium sulfate in 10 m*M* Tris–HCl buffer pH 8.5. The fractions containing the enzyme were combined and concentrated by ultramembrane filtration (Microcon YM3).

2.2. Crystallizations

Initial screening for crystallization of *Af*-HBDH was carried out using the hanging-drop vapour-diffusion method with the commercially available Crystal Screen and Crystal Screen II (Hampton Research Inc.) at room temperature and at 277 K. Crystals grew from several conditions, but only one that contained promising larger crystals was further optimized. Crystals suitable for X-ray experiments were grown within 2–3 d at 277 K when 2.0 µl droplets of protein solution containing 30 mg ml^{-1} enzyme in 50 m*M* Tris–HCl buffer pH 8.5 mixed with the same volume of reservoir solution were equilibrated against 1.0 ml reservoir solution containing 26–28%(*w*/*v*) PEG 4000 and 0.08–0.1 *M* lithium chloride or lithium sulfate. Two crystal forms (*Af*-HBDH-I and *Af*-HBDH-II) were obtained using lithium chloride and lithium sulfate, respectively. The best condition used a reservoir solution containing 28%(*w*/*v*) PEG 4000 and 0.1 *M* lithium chloride. Crystals of the enzyme in complex with NAD^+ and acetate (*Af*-HBDH–NAD–acetate) appeared within 2–3 d in hanging drops when 2 µl 20 mg ml^{-1} enzyme solution

Table 1
Crystal data and data-collection statistics.

Values in parentheses are for the highest resolution shell.

	Af-HBDH-I	*Af*-HBDH-II	*Af*-HBDH–NAD–acetate
Crystal data			
Beamline	AR-NW12	AR-NW12	BL 17A
Space group	$P2_1$	$P2_12_12_1$	$P4_12_12$
Unit-cell parameters			
a (Å)	77.3	82.5	91.4
b (Å)	118.8	118.8	91.4
c (Å)	118.7	121.2	262.1
β (°)	93.9		
Z†	8	4	4
Data collection			
Software	*HKL*-2000	*CrystalClear*	*CrystalClear*
Resolution (Å)	50–2.2 (2.3–2.2)	34.7–2.8 (2.9–2.8)	46.0–2.2 (2.3–2.2)
No. of observed reflections	387285	215288	716572
No. of unique reflections	107914 (10798)	57444 (5764)	57443 (5650)
Completeness (%)	98.9 (99.3)	99.7 (100)	100 (100)
$R_{\rm merge}$‡ (%)	7.6 (34.0)	5.0 (29.2)	13.3 (31.7)
Redundancy	3.6 (3.4)	3.7 (3.8)	12.5 (13.0)
$I/\sigma(I)$	37.8 (1.4)	12.5 (3.5)	12.3 (6.6)

† Number of subunits in the asymmetric unit. ‡ $R_{\rm merge} = 100 \times \sum_{hkl}\sum_i |I_i(hkl) - \langle I(hkl)\rangle| / \sum_{hkl}\sum_i I_i(hkl)$, where $I_i(hkl)$ is the *i*th measurement of the intensity of reflection *hkl* and $\langle I(hkl)\rangle$ is its mean value.

Table 2
Amino-acid identities (%) among related proteins that target a hydroxyl group of their substrate.

1, *Af*-HBDH; 2, (*S*)-1-phenylethanol reductase; 3, 3α,20β-hydroxysteroid dehydrogenase; 4, tropinone reductase; 5, sorbitol dehydrogenase; 6, alcohol dehydrogenase; 7, carbonyl reductase.

	1	2	3	4	5	6	7
2	35						
3	34	32					
4	34	29	30				
5	32	38	36	30			
6	30	25	23	23	26		
7	29	26	31	30	31	25	

containing 5 m*M* NAD^+ was mixed with an equal volume of mother liquor consisting of 30%(*w*/*v*) PEG 4000, 0.2 *M* sodium acetate trihydrate and 100 m*M* Tris–HCl pH 8.5 at 293 K.

2.3. X-ray data collection and processing

Crystals suitable for X-ray experiments were mounted in cryoloops with the respective reservoir solution containing 25% glycerol for 30 s and then flash-frozen in N_2 gas at 100 K for X-ray experiments. X-ray data for the *Af*-HBDH-I crystals were collected at 100 K on beamline AR-NW12 at the Photon Factory (Tsukuba, Japan) using synchrotron radiation of wavelength 1.00 Å. X-ray diffraction data were recorded on an ADSC Quantum 210 CCD detector positioned at a distance of 140 mm from the crystal. A total of 180 frames of diffraction were taken with 1° oscillation steps and 5 s exposure per frame. Bragg reflections were indexed and their intensities were integrated at 2.2 Å resolution using *HKL*-2000 (Otwinowski & Minor, 1997). Diffraction data for the *Af*-HBDH-II crystals were recorded as 360 frames with 0.5° oscillation steps and 5 s exposure per frame using the same detector system. The data for the *Af*-HBDH–NAD–acetate crystal were collected on Photon Factory beamline 17A (λ = 1.00 Å). 180 frames of diffraction with 1° oscillation steps and 5 s exposure were recorded on a Quantum ADSC 4R detector system at a distance of 244 mm from the crystal. The data were processed to 2.8 Å resolution for *Af*-HBDH-II and 2.2 Å resolution for the *Af*-HBDH–NAD–acetate complex using *CrystalClear* (Pflugrath, 1999). Relative intensities were scaled between the frames and converted to amplitudes using the program *TRUNCATE* from the *CCP*4 suite (Collaborative Computational Project, Number 4, 1994). The data observed from the crystals exhibited different extinction rules; from these, the space groups were determined to be $P2_1$ and $P2_12_12_1$ for the *Af*-HBDH-I and *Af*-HBDH-II crystals, respectively, and $P4_12_12$ for the *Af*-HBDH–NAD–acetate crystal. For these crystals, the calculated Matthews coefficients ($V_{\rm M}$; Matthews, 1968) and solvent contents (2.29 $Å^3\,Da^{-1}$ and 61.4% for *Af*-HBDH-I, 2.50 $Å^3\,Da^{-1}$ and 51.26% for *Af*-HBDH-II and 2.26 $Å^3\,Da^{-1}$ and 45.79% for the *Af*-HBDH–NAD–acetate complex, respectively) indicate that the asymmetric units contain eight subunits for *Af*-HBDH-I and four subunits for *Af*-HBDH-II and for the *Af*-HBDH–NAD–acetate complex. Crystal data and data-collection statistics are summarized in Table 1.

2.4. Sequence alignment

Prior to applying the molecular-replacement method for phase determination, homologous proteins with similar amino-acid sequences were surveyed in the PDB. Our idea was that the substrate of *Af*-HBDH was a type of carboxylic acid that also contained a hydroxyl group, as described in §1. Thus, the search also included enzymes whose substrates contain hydroxyl groups. The retrieved amino-acid sequences were correlated using a multiple-alignment technique with the program *Kalign* (Lassmann & Sonnhammer, 2006). Table 2 shows an amino-acid identity matrix between several proteins.

2.5. Structure determination and refinement

Three proteins (PDB codes 2ewm, 2hsd and 1ae1) showed high sequence identities, as shown in Table 2. Using these proteins as the structural probe for molecular replacement, phases were examined using the program *AMoRe* (Navaza, 1994) by changing the probe structures to monomeric, dimeric and tetrameric forms and by choosing data in several resolu-

Table 3
Structure-refinement statistics.

	Af-HBDH-I	*Af*-HBDH–NAD–acetate
Structure determination		
Resolution (Å)	50–2.2	40–2.2
Reflections used	60246	57435
R_{work}† (%)	19.7	19.1
R_{free}‡ (%)	27.0	23.6
No. of protein atoms	15248	7624
Water molecules	400	831
NAD^+ molecules	—	4
Acetate ions	—	4
Ca^{2+} ions	4	2
Cl^- ions	8	4
Root-mean-square deviations		
Bond lengths (Å)	0.007	0.005
Bond angles (°)	1.3	1.2
Ramachandran plot		
Residues in most favoured regions (%)	90.9	91.3
Residues in additionally allowed regions (%)	9.0	8.7
Residues in generously allowed regions (%)	0.1	0.0
Residues in disallowed regions (%)	0.0	0.0

† $R_{work} = 100 \times \sum ||F_o| - |F_c|| / \sum |F_o|$, where $|F_o|$ and $|F_c|$ are the observed and calculated structure-factor amplitudes, respectively. ‡ Calculated using a random set containing 10% of observations that were not included throughout refinement (Brünger, 1992).

tion ranges. When the tetrameric structure of 2hsd (3α,20β-hydroxysteroid dehydrogenase from *Streptomyces hydrogenas*; Ghosh *et al.*, 1994) was used, a significant solution was found with a high CC value (43.6%) and a low *R* value (45.4%). The constructed crystal structure indicated reasonable molecular packing. The correctness of the solution was subsequently confirmed by a similar calculation using the *Pf*-HBDH structure (Ito *et al.*, 2006). An electron-density map calculated based on this solution and averaged among the eight subunits showed sufficient quality to allow not only the side-chain replacements, but also the insertion and deletion of amino-acid residues in the eight subunits of *Af*-HBDH-I.

The atomic parameters of the constructed structures were initially refined by the rigid-body and restrained maximum-likelihood least-squares technique using the program *REFMAC*5 from the *CCP*4 program suite (French & Wilson, 1978; Collaborative Computational Project, Number 4, 1994). In the initial stage of refinement the eight subunits were presumed to be identical with noncrystallographic symmetry, but this subunit constraint was released in subsequent refinement. After several cycles of *REFMAC* refinement, crystallographic conjugate-gradient minimization and *B*-factor refinement were performed with the program *CNS* (Brünger *et al.*, 1998). The structure was revised by interpreting OMIT maps at each residue using the program *QUANTA* (Accelrys Inc.). Water molecules were assigned using the water-picking routine of *CNS*. Some of them were assigned as Ca^{2+} and Cl^- ions in structural refinement because their densities were higher than those of other water O atoms. The structure was analyzed by *PROCHECK* (Laskowski *et al.*, 1993) at each step of both *REFMAC*5 and *CNS* refinement. Molecular replacement of *Af*-HBDH-II gave a unique solution (CC value of 76.3% and *R* value of 37.0%) in space group $P2_12_12_1$ when the tetramer of *Af*-HBDH-I was used as a search model. The initial structure was not further refined because of its low-resolution diffraction data in comparison with *Af*-HBDH-I.

The initial structure of the *Af*-HBDH–NAD–acetate crystal was also solved by molecular replacement with *AMoRe* using the refined *Af*-HBDH-I tetramer as a model. The NAD^+ cofactors were clearly located in the electron-density map and were added to the structural refinement. Geometric restraints for the cofactor were prepared using the HIC-Up server (http://xray.bmc.uu.se/hicup/). Electron density for an acetate anion was found in the active site. Furthermore, electron densities for Ca^{2+} and Cl^- ions were also found at sites corresponding to those of *Af*-HBDH-I. The final structural refinements including these ions and water molecules were performed in a similar manner as described above with the programs *REFMAC* and *CNS*. Statistics of the structure determination are given in Table 3.

The atomic coordinates were deposited in the PDB (codes 2yz7 and 2zea). All visualization and image production was performed with *RASMOL* (Sayle & Milner-White, 1995) and

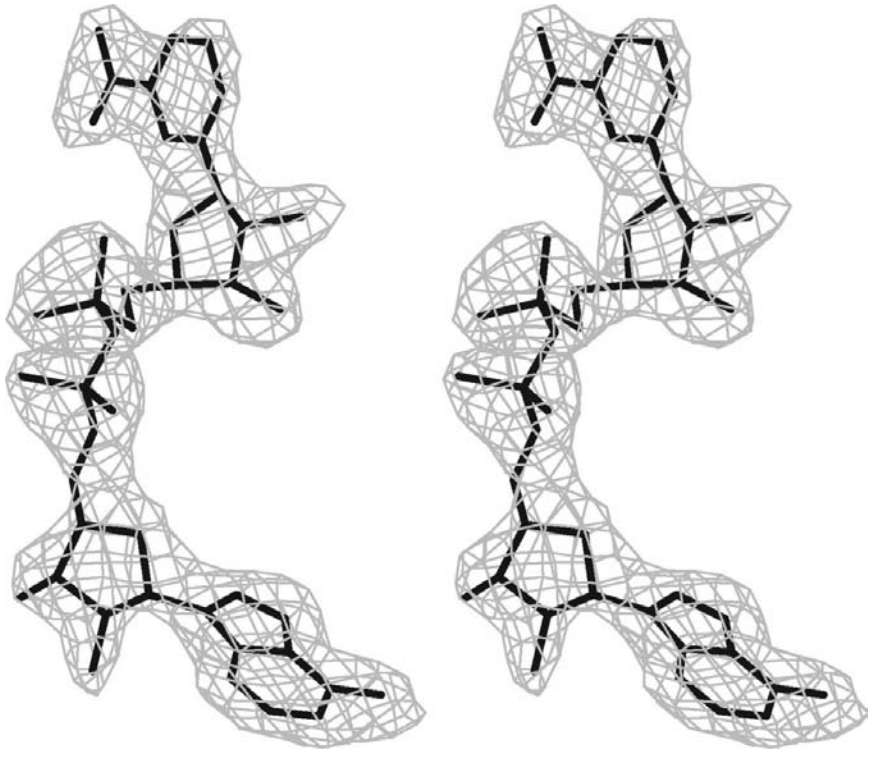

Figure 2
A stereoview of a $|F_o| - |F_c|$ OMIT map of NAD^+ in the *Af*-HBDH–NAD–acetate complex crystal. Contours are drawn at the 2.5σ level.

PyMOL (DeLano Scientific; http://www.pymol.org). The topological diagram was drawn using *TopDraw* (Bond, 2003). Fig. 2 shows an $|F_o| - |F_c|$ OMIT map drawn using the program *O* (Jones *et al.*, 1991). Sequence alignments were performed with *Kalign* (Lassmann & Sonnhammer, 2006). Structural comparisons were carried out using *Swiss-Pdbviewer* (http://www.expasy.org/spdbv/).

3. Results and discussion

3.1. Quality of the structure

The *Af*-HBDH-I crystal diffracted well to 2.2 Å resolution. The crystal structure was refined resulting in a crystallographic *R* factor of 19.7% (R_{free} = 27.0% for 10% of the observed data that were not included throughout refinement). The final refined structure contains eight subunits (*A*–*H*) with 260 amino acids in each, eight chloride ions, four calcium ions and 400 water molecules in the asymmetric unit. *Af*-HBDH is tetrameric with noncrystallographic 222 symmetry. Almost all of the residues are well defined in the electron-density map. The eight subunits are structurally similar to each other, with root-mean-square (r.m.s.) deviations of 0.5–0.6 Å between the corresponding C^{α} atoms (comparing the *A* subunit with subunits *B*–*H*), indicating that they are essentially identical. Their Ramachandran plots (Ramachandran *et al.*, 1963) show that all of the main-chain atoms fall within the allowed regions, with 90.9% of residues in the most favoured regions, 9.0% of residues in additionally allowed regions and 0.1% of residues in generously allowed regions.

The crystal structure of the *Af*-HBDH–NAD–acetate complex was refined to an *R* factor of 19.1% (R_{free} = 23.6%) for all observed data without any cutoff in the resolution range 40–2.2 Å (Table 3). There are four subunits, four NAD^+ molecules, four acetate ions, four chloride ions, two calcium ions and 831 water molecules in the asymmetric unit. The electron density was well defined over the entire structure in the *Af*-HBDH–NAD–acetate complex. The peptide folds of the four subunits are similar to each other, with an r.m.s. deviation of 0.2–0.3 Å between corresponding C^{α} atoms. A Ramachandran plot of the four polypeptides shows that all of the main-chain atoms fall within the allowed regions, with 91.3% of residues in the most favoured regions and 8.7% of residues in additionally allowed regions.

In both crystal forms, the calcium ion is coordinated by two C-terminal carboxyl groups together with four water molecules at distances in the range 2.4–2.6 Å. Characteristically, a calcium ion is seven-coordinate; in this case, one coordination is missing (it is occupied by the hydrophobic side chain of a Val residue). The refined temperature factors of the calcium ions are also reasonable at around 24 $Å^2$. The locations of the Ca^{2+} ions are between the two subunits of the tetramer. It seems that they are essential for stabilization of the tetramer. Therefore, the bound Ca^{2+} ions might be retained during purification. The bound chloride ions may come from the buffer solution.

3.2. Overall fold and subunit structure

A stereo diagram of the tetrameric apo HBDH (*Af*-HBDH-I) structure is shown in Fig. 3. The two tetramers in the asymmetric unit have similar structures, with an r.m.s. deviation of 0.7 Å between corresponding C^{α} atoms. HBDH thus displays the prototypical quaternary arrangement observed in several SDRs (*e.g.* bacterial 3α/20β-hydroxysteroid dehydrogenase, rat type II hydroxyacyl-CoA dehydrogenase or mouse lung carbonyl reductase; Powell *et al.*, 2000; Ghosh *et al.*, 1991; Tanaka *et al.*, 1996). Only for residues 190–215 is the electron density not well defined in several subunits, most likely as a consequence of the loose crystal packing. However, one subunit has better density for these regions and therefore this structure is considered in the following to be representative of the eight subunits.

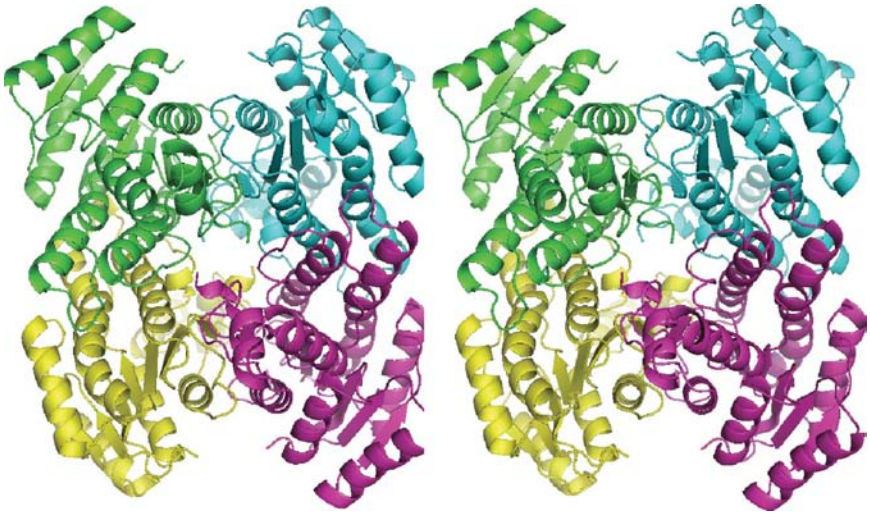

Figure 3
The molecular structure of HBDH from *A. faecalis*. A stereo ribbon-cartoon diagram shows the tetrameric architecture as the biological unit, which is formed from four subunits (each drawn in different colour) with noncrystallographic 222 symmetry. There are two independent tetramers in the asymmetric unit of the *Af*-HBDH-I crystal.

The structural features of apo HBDH are maintained in the *Af*-HBDH–NAD–acetate complex. Superimposition of corresponding C^{α} atoms gave r.m.s.d. values of less than 0.4 Å, suggesting that the binding of NAD^+ has little effect on the peptide folding. Therefore, the structural features of the *Af*-HBDH–NAD–acetate complex are discussed in the following. The core of each subunit contains an open α/β motif: the well known Rossmann fold that is common to SDR-family enzymes. The central β-sheet consists of seven parallel β-strands (S1–S7) and is sandwiched by three α-helices on each side (H1, H2 and H8 on one side and H3, H4 and H5 on the other) to form the

principal domain of the subunit. A stereo ribbon representation of the secondary structure of HBDH in complex with NAD^+ and acetate is shown in Fig. 4(*a*). The β-sheet is twisted in a left-handed pattern as is commonly observed. Three helices on either side of the sheet are bundled with a left-handed twist. An additional two helices, H6 and H7, are extruded to form another small domain. A topological diagram of the secondary structure is shown in Fig. 4(*b*). There is a cleft at the C-terminal edge of the β-strands of the principal domain in which an NAD^+ molecule is accommodated. The small additional domain covers the cleft. In the *Af*-HBDH–NAD–acetate complex, however, the electron-density map of the small domain (residues 190–215) is well defined. The two extended arms (185–190 and 196–227) seem to be hinged to the principal domain, allowing movement of the small domain. Although *Pf*-HBDH (Ito *et al.*, 2006) and DHRS6 (Guo *et al.*, 2006) have sequence identities of 72% and 31% to *Af*-HBDH, respectively, their folding patterns are almost identical, with r.m.s. deviations of 0.6 and 1.3 Å for corresponding C^α atoms, respectively.

3.3. NAD^+-binding region

The binding site for NAD^+ in the *Af*-HBDH–NAD–acetate complex is shown in Fig. 5. The final OMIT map is well defined for all parts of the coenzyme (Fig. 1). In each subunit, NAD^+ binds in an extended conformation, with the distance between the C2 atom of the nicotinamide ring in the *syn* conformation and the C6 atom of the adenine moiety in the *anti* conformation being 14.0 Å. Both ribose rings adopt a C2′ *endo* (^{2}E) conformation. The NAD^+-binding geometry is similar to those found in previously reported structures of the SDR family (Varughese *et al.*, 1992; Benach *et al.*, 1999; Guo *et al.*, 2006).

The bound NAD^+ is surrounded by residues 11, 14–17, 34, 36, 62, 64, 90–94, 113, 152, 185–188 and 190–192 and the catalytic residues Ser142, Tyr155 and Lys159. The nicotinamide moiety is accommodated in a hydrophobic pocket composed of Ile16, Ile140, Pro185, Val188 and Val193. The carbamoyl group is anchored by the main-chain amide N atom and the carbonyl O atoms of Val188 and the side-chain O atom of Thr190 (Fig. 5). These wide interactions result in the exposure of the *B* face of the nicotinamide ring towards the void space of the cleft, which leads to the observed specificity for pro-*S* hydride transfer of the substrate D-3-hydroxybutyrate (Hashimoto *et al.*, 1992). Furthermore, the 2′-OH group of the nicotinamide nucleotide forms two hydrogen bonds to Tyr155 and Lys159 and the 3′-OH group forms hydrogen bonds to Lys159 and the main-chain carbonyl of Asn90. The loop between S1 and H1 contains a consensus sequence G*XXX*G*X*G that is typical of the SDR family (Jörnvall *et al.*, 1995). It interacts with the pyrophosphate moiety through a hydrogen bond to the main-chain NH group of Ile16. The pyrophosphate further interacts with Thr190 and with two water molecules. The adenine ring is

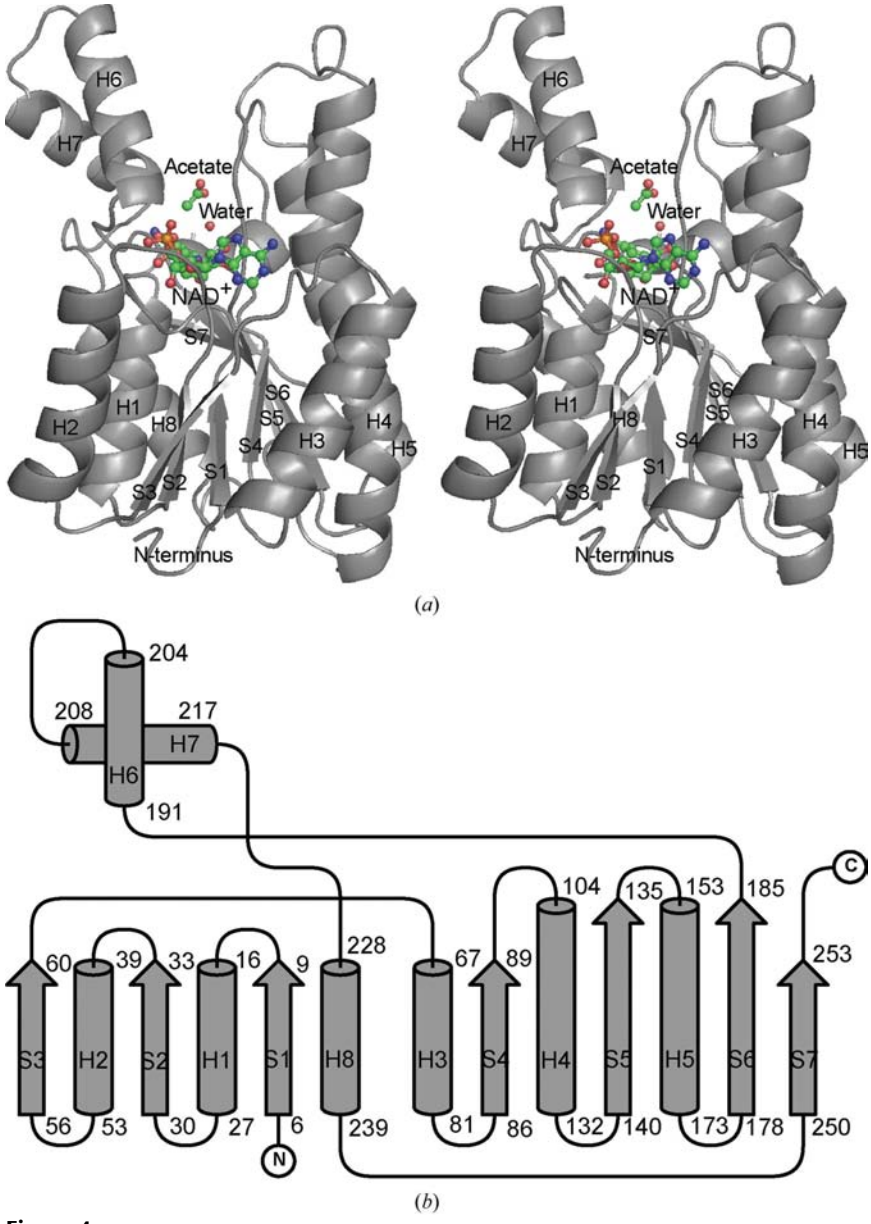

Figure 4
The architecture of a subunit of the tetrameric *Af*-HBDH–NAD–acetate complex. (*a*) A stereo ribbon-cartoon drawing of one of the four subunits in the asymmetric unit. The NAD^+, acetate and water molecules are shown in ball-and-stick representation. (*b*) A topological diagram of the secondary structure. The secondary structure was assigned with the program *PROCHECK* (Laskowski *et al.*, 1993). Strands and helices are represented by arrows and cylinders, respectively. The principal domain adopts an open α/β structure containing a typical Rossmann fold, in which the seven β-strands are all parallel to each other. At the centre, a topological switching point is formed between strands S1 and S4 for the catalytic site.

packed in a hydrophobic pocket comprised of Asn34, Phe36, Leu64, Ala91, Ile93 and Leu113. The amino group of the adenine moiety forms a hydrogen bond to Asp63. The O2′ atom of the adenosine nucleotide forms a hydrogen bond to the main-chain NH of Phe36, whereas the O3′ atom forms hydrogen bonds to Thr13 and Ser14. The NAD^+ molecule is thus entirely fitted into the surface groove generated by the enzyme. These NAD^+-binding features are similar to those described by Duax *et al.* (2003).

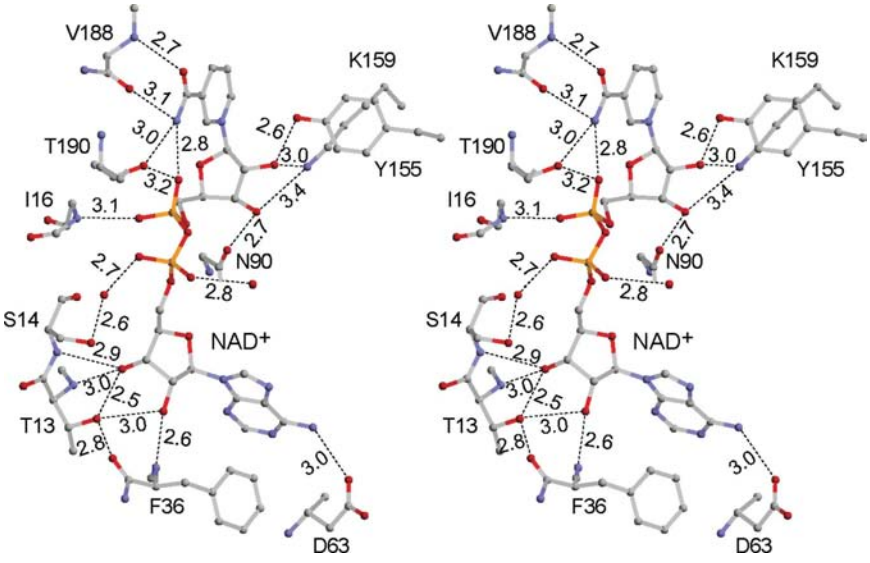

Figure 5
NAD^+-binding geometry in *Af*-HBDH. Possible hydrogen bonds are indicated by broken lines, except for hydrogen bonds to water molecules. The bound NAD^+ molecule is shown in ball-and-stick representation. Values indicate distances in angstroms for the *A* subunit.

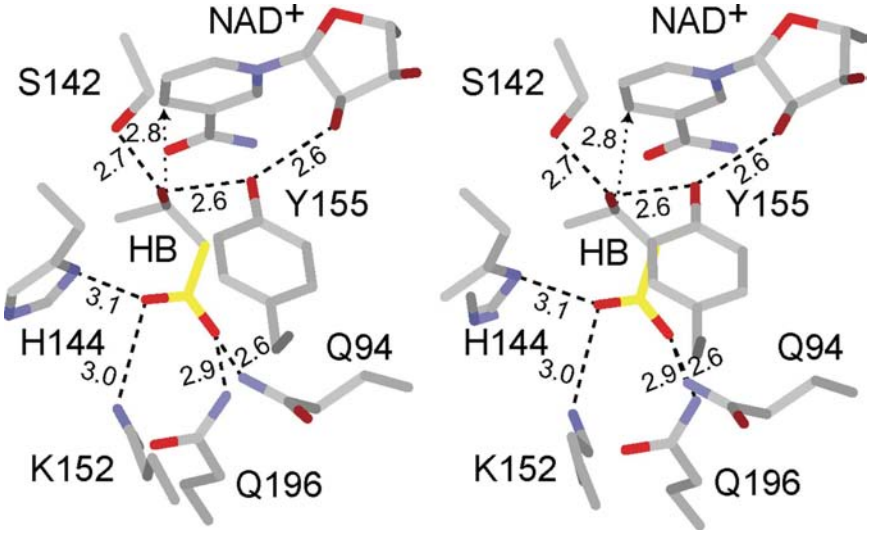

Figure 6
A D-3-hydroxybutyrate-bound model of *Af*-HBDH constructed by adding two C atoms around the bound acetate and water molecules. The acetate carboxyl group forms hydrogen bonds from one O atom to His144 and Lys152, while the other O atom forms hydrogen bonds to Gln94 and Gln196 (see text). The bound acetate molecule is highlighted in yellow. Positioning the β-carbon in the *R* configuration results in a close contact with the C4 atom of the cofactor (2.8 Å) to facilitate its hydride donation. Hydrogen bonds are shown by broken lines with lengths in angstroms.

In the *Af*-HBDH–NAD–acetate complex, the second small domain is moved closer to the principal domain to trap NAD^+ in the cleft by an opening/closing mechanism[1]. This movement may induce partial ordering of the substrate-binding loop, which is stabilized through hydrogen bonds between the main-chain NH of Val188 and the amide group of NAD^+ and between the hydroxyl group of Thr190 and the 5′-phosphate group of the nicotinamide nucleotide. Therefore, those interactions might facilitate the opening/closing movement in substrate binding as described below.

3.4. Acetate binding suggests the substrate binding

Inspection of $2|F_o| - |F_c|$ and $|F_o| - |F_c|$ maps during refinement showed the presence of strong residual density with a triangular shape near the active site in each subunit. Sodium acetate trihydrate was added to the crystallization solution and the residual density probably corresponds to acetate ion. Acetate binding occurs just above the nicotinamide moiety in the entrance pocket of a tunnel formed by the H6 helix and three loops (S4–H4, S6–H6 and the C-terminus) of the *Af*-HBDH–NAD–acetate complex. It is easy to see how the movement of H6 on NAD^+ binding is essential for substrate binding. The carboxyl group of the acetate ion is bound to the side chains of His144, Lys152, Gln94 and Gln196 by hydrogen bonds of lengths 3.1, 3.0, 2.6 and 2.9 Å, respectively. These are the substrate-specific residues of HBDH and they are conserved in the 27 surveyed HBDHs. A water molecule is trapped in the catalytic centre through hydrogen bonds to the acetate carboxyl group and the side chains of Ser142 and Tyr155 (2.9, 2.6 and 2.6 Å, respectively). The water molecule is positioned at a distance of 3.4 Å from the C4 atom of the nicotinamide ring of NAD^+. This situation suggests that the water molecule takes the place of the hydroxyl group of the real substrate. When a C atom is added at the β position between the water and the methyl group of the bound acetate, it is easy to generate a model of β-hydroxypropionate. Furthermore, by adding another C atom at the γ position with the *R* configuration, D-3-hydroxybutylate can reason-

[1] In the apoenzyme, the temperature factors of these residues are relatively high with a wide range in the eight subunits depending on the crystal packing. Such flexibility of the domain has been exemplified in the crystal structure of *Pseudomonas putida* HBDH (Paithankar *et al.*, 2007), which was published just before the submission of our manuscript.

ably be constructed as a bound substrate without any atomic conflicts[2], as shown in Fig. 6. In this model, the C^{β} atom is positioned at a distance of 2.8 Å facing towards the C4 atom of the nicotinamide ring (the H atom attached to the C^{β} atom is at a distance of 1.9 Å). This arrangement could reasonably facilitate hydride transfer to the C4 atom of NAD^{+}.[3]

3.5. Catalytic reaction mechanism

Based on the model proposed above, the reaction mechanism of HBDH can be elucidated. Two residues, Ser142 and Tyr155, play essential roles in catalysis. At the optimal pH (8.5), it is plausible to assume that Tyr155 is deprotonated because the pK_a value of tyrosine (10.1) is lower than that of serine (13.0). Therefore, the Ser142 residue donates an H atom for the formation of a hydrogen bond to the hydroxyl group of the substrate and the Tyr155 residue accepts an H atom from the hydroxyl group. When the hydroxyl group is fixed between Ser142 and Tyr155, the ionized Tyr155 will easily withdraw a proton from the hydroxyl group. This process facilitates carbonyl-bond formation in the substrate. At the same time, the H atom attached to the β-carbon is transferred to the C4 atom of the nicotinamide ring of the bound NAD^{+}. It is noted that the Lys159 residue has two possible roles. The first is to assist the proper orientation of the coenzyme by forming hydrogen bonds to the O atoms of the nicotinamide-ribose moiety and the second is to lower the pK_a value of Tyr155 by an electrostatic effect. A proposed reaction mechanism is illustrated in Fig. 7. The Tyr/Lys mechanism would constitute an explanation of the strict conservation and appears to be compatible with much of the known data (Jörnvall *et al.*, 1995).

3.6. Evolutionary conservation and biological implications

Many three-dimensional structures of proteins belonging to the SDR family have previously been solved by X-ray crystallography (Oppermann *et al.*, 2003). As shown in Table 2, their sequence identities

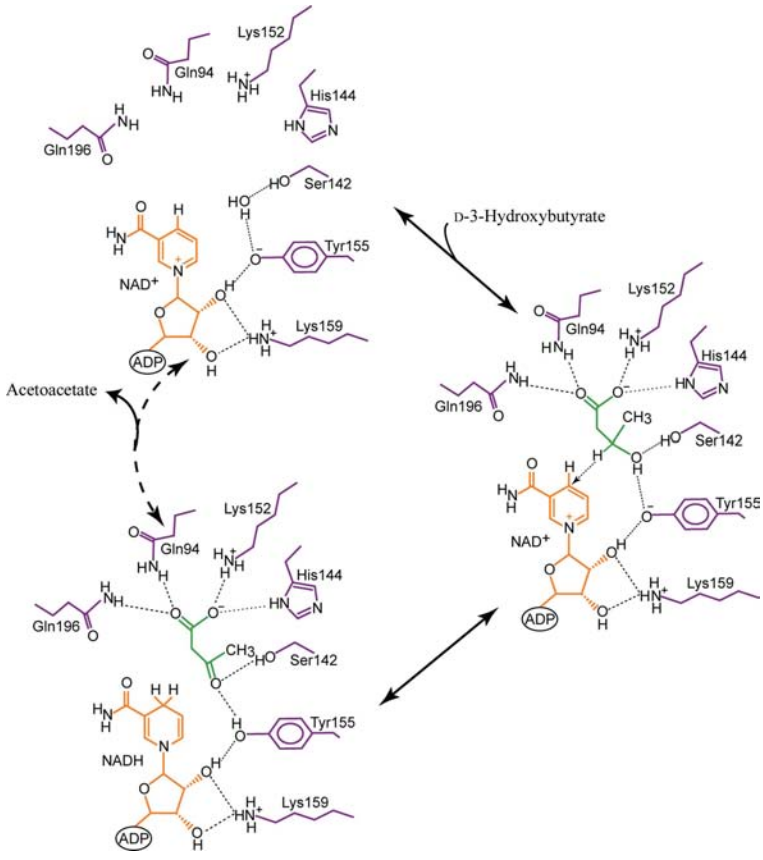

Figure 7
Proposed catalytic reaction mechanism of HBDH.

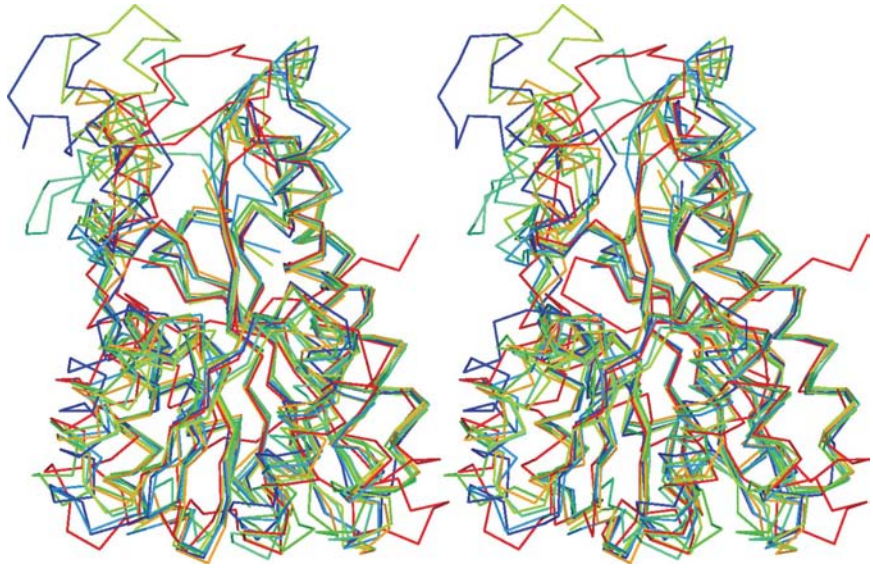

Figure 8
Structural comparison of several related enzymes from the SDR family. A stereo diagram shows the C^{α} traces of (*S*)-1-phenylethanol reductase from the denitrifying bacterium strain EbN1 (blue, PDB code 2ewm; Hoffken *et al.*, 2006), 3α,20β-hydroxysteroid dehydrogenase from *Streptomyces hydrogenas* (light blue, PDB code 2hsd; Ghosh *et al.*, 1994), tropinone reductase I from *Datura stramonium* (cyan, PDB code 1ae1; Nakajima *et al.*, 1998), sorbitol dehydrogenase from *Rhodobacter sphaeroides* (yellow, PDB code 1k2w; Philippsen *et al.*, 2005), carbonyl reductase from mouse lung (orange, PDB code 1cyd; Tanaka *et al.*, 1996) and alcohol dehydrogenase from *Drosophila melanogaster* (red, PDB code 1mg5; Benach *et al.*, 2005). They are superimposed onto that of the *Af*-HBDH–NAD–acetate complex (green). The principal domains are highly conserved, but the small domains differ for the generation of wide substrate specificity.

[2] An alternative methyl C atom with the *S* configuration is difficult to accommodate in the enzyme.

[3] The substrate-bound model proposed by Paithankar *et al.* (2007) is absolutely inconsistent with our observed structure.

are generally low (23–35%), even in the N-terminal and central regions, but their peptide folds are similar to each other. The highest similarity can be seen in the Rossmann fold, whereas the most variable parts are found in the substrate-recognition site as the substrates are widely spread from the simplest alcohol to complex compounds such as steroids, prostaglandins, sugars and xenobiotics. In every case, however, they catalyze a similar reaction scheme of keto/hydroxyl interconversion. When the C^{α} atoms of their subunits are superimposed onto those of *Af*-HBDH–NAD–acetate (Fig. 8), the main chains are folded with the same topology (the corresponding C^{α}-atom r.m.s.d.s are in the range 1.1–1.5 Å). The tertiary structures of their principal domains are highly conserved, whereas the most variable regions are found in the small additional domains. Remarkable differences occur in the loop regions between S2 and H2 and between S6 and H8. In the latter, H6 and H7 are involved in coenzyme and substrate binding. The low sequence homology of this region is consistent with the variety of substrate specificity. The long loop region between S6 and H8 in alcohol dehydrogenase is in close contact with the loop connecting S4 and H4 because of its small substrate. Additional structural differences are found in a subset of the short-chain dehydrogenase family that use the cofactor NADP(H) rather than NAD(H). The essential signature of this family is the appearance of a Y*XXX*K motif that is strictly conserved. Our structure determination reveals that the invariant tyrosine and lysine residues are located in the catalytic pocket and are involved in the reaction. A third residue, Ser, is also conserved in HBDH as well as in the SDR family, forming a Ser-Tyr-Lys catalytic triad in the active site that might be responsible for a hydride transfer and a proton transfer. These catalytic residues are also found in similar positions in other SDR-type dehydrogenases (Jörnvall *et al.*, 1995; Filling *et al.*, 2002). Thus, it can be concluded that these enzymes developed in evolutionary divergence to form a wide variety of SDR family members from a common ancestor protein by conserving the catalytic site and changing the substrate-recognition site.

We thank N. Igarashi and S. Wakatsuki for help with data collection. This work was supported in part by Grants-in-Aid for the Protein 3000 Project for Metabolic Proteins (S. Kuramitsu) from the Ministry of Education, Culture, Sports, Science and Technology of Japan.

References

Benach, J., Atrian, S., Gonzalez-Duarte, R. & Ladenstein, R. (1999). *J. Mol. Biol.* **289**, 335–355.
Benach, J., Winberg, J., Svendsen, J., Atrian, S., Gonzalez-Duarte, R. & Ladenstein, R. (2005). *J. Mol. Biol.* **345**, 579–598.
Bond, C. S. (2003). *Bioinformatics*, **19**, 311–312.
Brünger, A. T. (1992). *Nature (London)*, **355**, 472–475.
Brünger, A. T., Adams, P. D., Clore, G. M., DeLano, W. L., Gros, P., Grosse-Kunstleve, R. W., Jiang, J.-S., Kuszewski, J., Nilges, M., Pannu, N. S., Read, R. J., Rice, L. M., Simonson, T. & Warren, G. L. (1998). *Acta Cryst.* D**54**, 905–921.
Collaborative Computational Project, Number 4 (1994). *Acta Cryst.* D**50**, 760–763.
Duax, W. L., Pletnev, V., Addlagatta, A., Bruenn, J. & Weeks, C. M. (2003). *Proteins*, **53**, 931–943.
Filling, C., Berndt, K. D., Benach, J., Knapp, S., Prozorovski, T., Nordling, E., Ladenstein, R., Jörnvall, H. & Oppermann, U. (2002). *J. Biol. Chem.* **277**, 25677–25684.
Francois, B., Bachmann, C. & Schutgens, R. (1981). *J. Inherit. Metab. Dis.* **4**, 163–164.
French, S. & Wilson, K. (1978). *Acta Cryst.* A**34**, 517–525.
Ghosh, D., Wawrzak, Z., Weeks, C. M., Duax, W. L. & Erman, M. (1994). *Structure*, **2**, 629–640.
Ghosh, D., Weeks, C. M., Grochulski, P., Duax, W. L., Erman, M., Rimsay, R. L. & Orr, J. C. (1991). *Proc. Natl Acad. Sci. USA*, **88**, 10064–10068.
Guo, K., Lukacik, P., Papagrigoriou, E., Meier, M., Lee, W. H., Adamski, J. & Oppermann, U. (2006). *J. Biol. Chem.* **281**, 10291–10297.
Hashimoto, T., Nakajima, K., Ongena, G. & Yamada, Y. (1992). *Plant Physiol.* **100**, 836–845.
Hoffken, H. W., Duong, M., Friedrich, T., Breuer, M., Hauer, B., Reinhardt, R., Rabus, R. & Heider, J. (2006). *Biochemistry*, **45**, 82–93.
Ikeda, T., Yoshida, T., Ito, Y., Murakami, I., Mokuda, O., Tominaga, M. & Mashiba, H. (1987). *Arch. Biochem. Biophys.* **257**, 140–143.
Ito, K., Nakajima, Y., Ichihara, E., Ogawa, K., Katayama, N., Nakashima, K. & Yoshimoto, T. (2006). *J. Mol. Biol.* **355**, 722–733.
Jain, S. K., Kannan, K. & Lim, G. (1998). *Free. Radic. Biol. Med.* **25**, 1083–1088.
Jones, T. A., Zou, J.-Y., Cowan, S. W. & Kjeldgaard, M. (1991). *Acta Cryst.* A**47**, 110–119.
Jörnvall, H., Persson, B., Krook, M., Atrian, S., Gonzalez-Duarte, R., Jeffery, J. & Ghosh, D. (1995). *Biochemistry*, **34**, 6003–6013.
Kallberg, Y., Oppermann, U., Jörnvall, H. & Persson, B. (2002). *Protein Sci.* **11**, 636–641.
Kruger, K., Lang, G., Weidner, T. & Engel, A. M. (1999). *Appl. Microbiol. Biotechnol.* **52**, 666–669.
Laffel, L. (1999). *Diabetes Metab. Res. Rev.* **15**, 412–426.
Laskowski, R. A., MacArthur, M. W., Moss, D. S. & Thornton, J. M. (1993). *J. Appl. Cryst.* **26**, 283–291.
Lassmann, T. & Sonnhammer, E. L. (2006). *Nucleic Acids Res.* **34**, W596–W599.
Malaisse, W. J., Lebrun, P., Yaylali, B., Camara, J., Valverde, I. & Sener, A. (1990). *Am. J. Physiol.* **259**, E117–E122.
Matthews, B. W. (1968). *J. Mol. Biol.* **33**, 491–497.
Nakajima, K., Yamashita, A., Akama, H., Nakatsu, T., Kato, H., Hashimoto, T., Oda, J. & Yamada, Y. (1998). *Proc. Natl Acad. Sci. USA*, **95**, 4876–4881.
Navaza, J. (1994). *Acta Cryst.* A**50**, 157–163.
Oppermann, U., Filling, C., Hult, M., Shafqat, N., Wu, X., Lindh, M., Shafqat, J., Nordling, E., Kallberg, Y., Persson, B. & Jörnvall, H. (2003). *Chem. Biol. Interact.* **143**, 247–253.
Otwinowski, Z. & Minor, W. (1997). *Methods Enzymol.* **276**, 307–326.
Paithankar, K. S., Feller, C., Kuettner, E. B., Keim, A., Grunow, M. & Strater, N. (2007). *FEBS J.* **274**, 5767–5779.
Pflugrath, J. W. (1999). *Acta Cryst.* D**55**, 1718–1725.
Philippsen, A., Schirmer, T., Stein, M. A., Giffhorn, F. & Stetefeld, J. (2005). *Acta Cryst.* D**61**, 374–379.
Powell, A. J., Read, J. A., Banfield, M. J., Gunn-Moore, F., Yan, S. D., Lustbader, J., Stern, A. R., Stern, D. M. & Brady, R. L. (2000). *J. Mol. Biol.* **303**, 311–327.
Ramachandran, G. N., Ramakrishnan, C. & Sasisekharan, V. (1963). *J. Mol. Biol.* **7**, 95–99.
Randle, P. J., Newsholme, E. A. & Garland, P. B. (1964). *Biochem. J.* **93**, 652–665.
Sayle, R. & Milner-White, E. J. (1995). *Trends Biochem. Sci.* **20**, 374.
Tanaka, N., Nonaka, T., Nakamura, K. T. & Deyashiki, Y. (2001).

Curr. Org. Chem. **5**, 89–111.
Tanaka, N., Nonaka, T., Nakanishi, M., Deyashiki, Y., Hara, A. & Mitsui, Y. (1996). *Structure*, **4**, 33–45.
Varughese, K. I., Skinner, M. M., Whitely, J. M., Matthews, D. A. & Xuong, N.-H. (1992). *Proc. Natl Acad. Sci. USA.* **89**, 6080–6084.